Electronic Supplementary Information (ESI) for

Bandgap Modification in 0D Tellurium Iodide Perovskite Derivatives via Incorporation of Polyiodide Species

Benjamin W. Walusiak,[1] Adharsh Raghavan,[1] Christopher L. Cahill[1]

[1]Departent of Chemistry, The George Washington University, 800 22nd Street, NW, Washington, D.C. 20052, United States

Email: cahill@gwu.edu

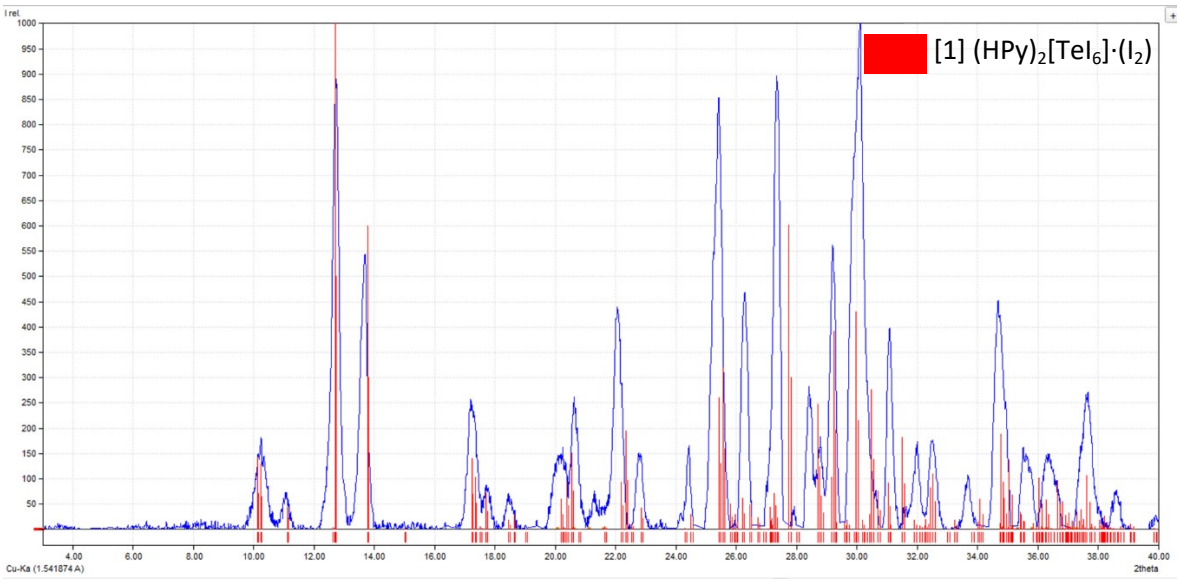

Figure S1. PXRD of **1** $(HPy)_2[TeI_6]\cdot(I_2)$, with the calculated pattern is overlaid red. This preparation of **1** followed the method utilizing stabilized HI detailed in the main manuscript, resulting in a much more predictable synthesis (in contrast to Figure S1.)

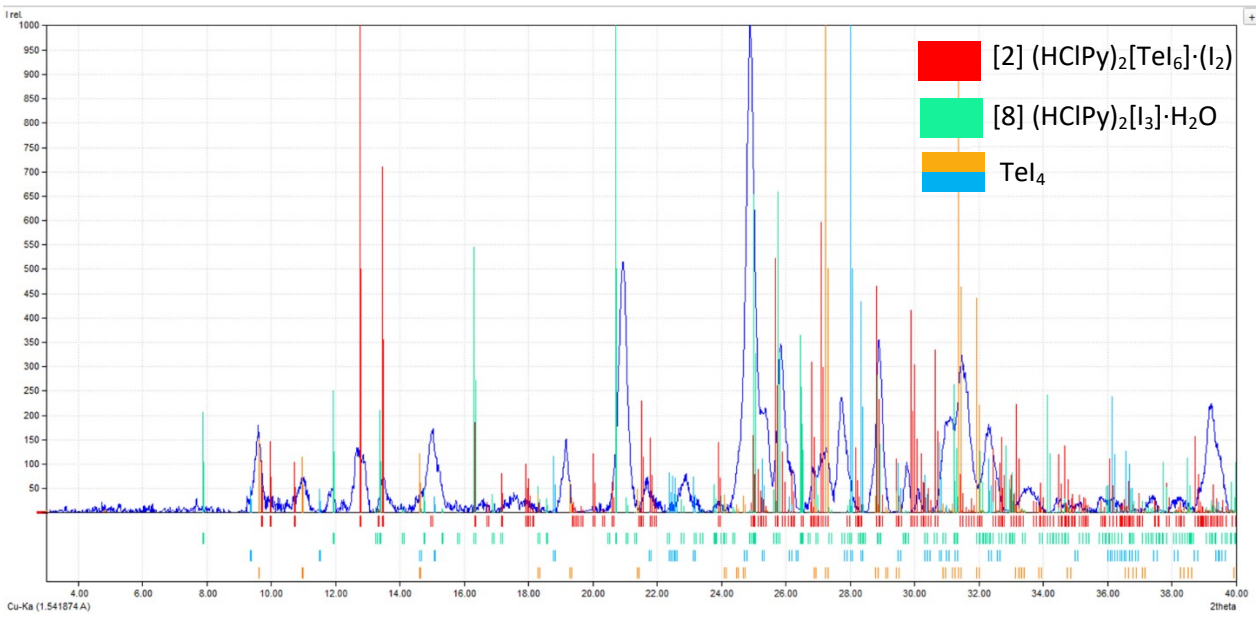

Figure S2. PXRD of **2** $(HClPy)_2[TeI_6]\cdot(I_2)$, with the calculated pattern is overlaid red. **8** $(ClPy)[I_3]\cdot H_2O$ is also present, overlaid in green. Tellurium iodide accounts for the remaining peaks (blue, orange).

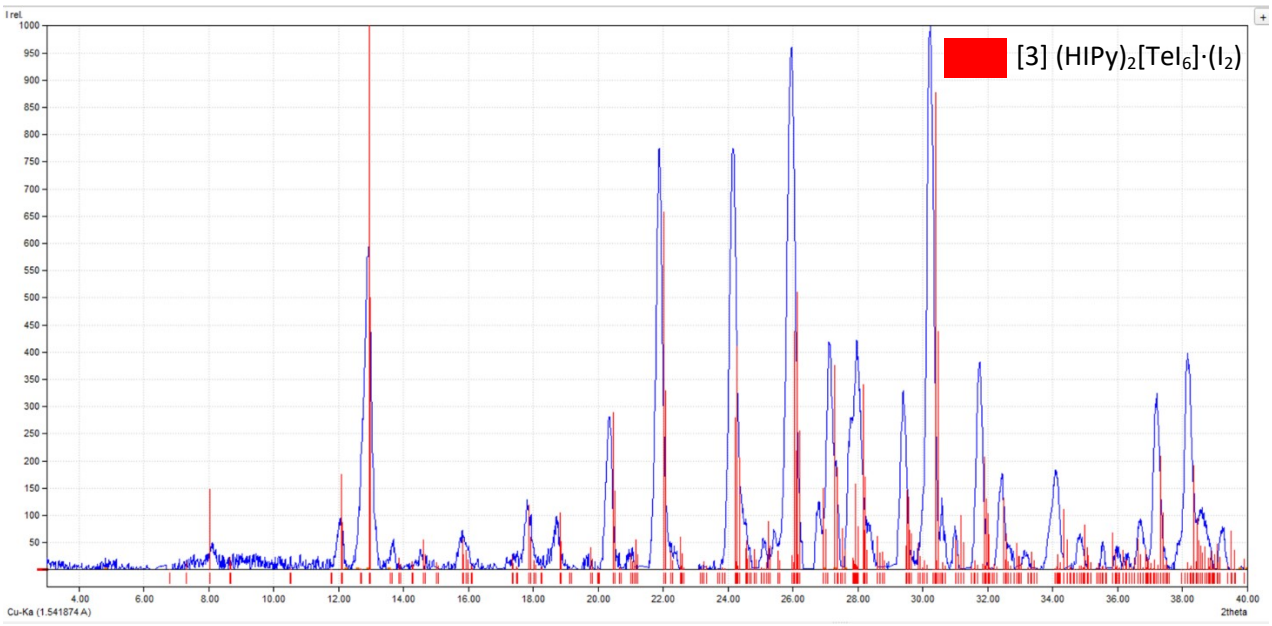

Figure S3. PXRD of **3** $(HIPy)_2[TeI_6]\cdot(I_2)$, with the calculated pattern overlaid red.

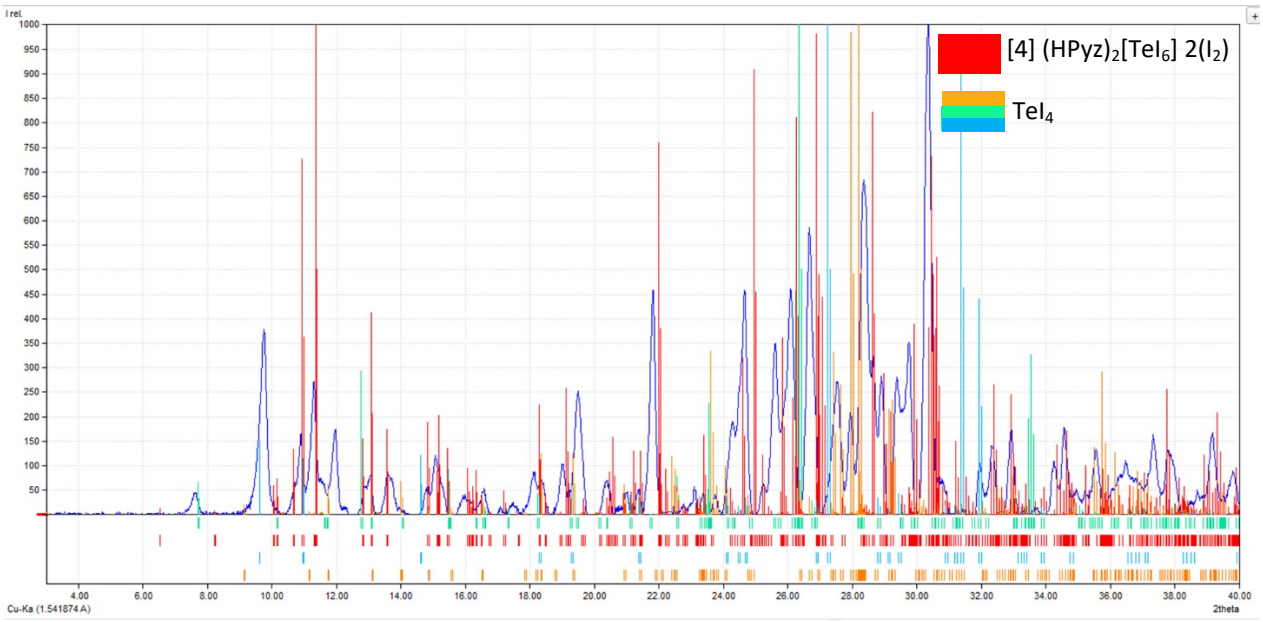

Figure S4. PXRD of **4** $(HPyz)_2[TeI_6]\cdot 2(I_2)$. The calculalted pattern for **4** is shown in red. Other peaks are accounted for by various TeI_4 phases (light blue, orange, and green)

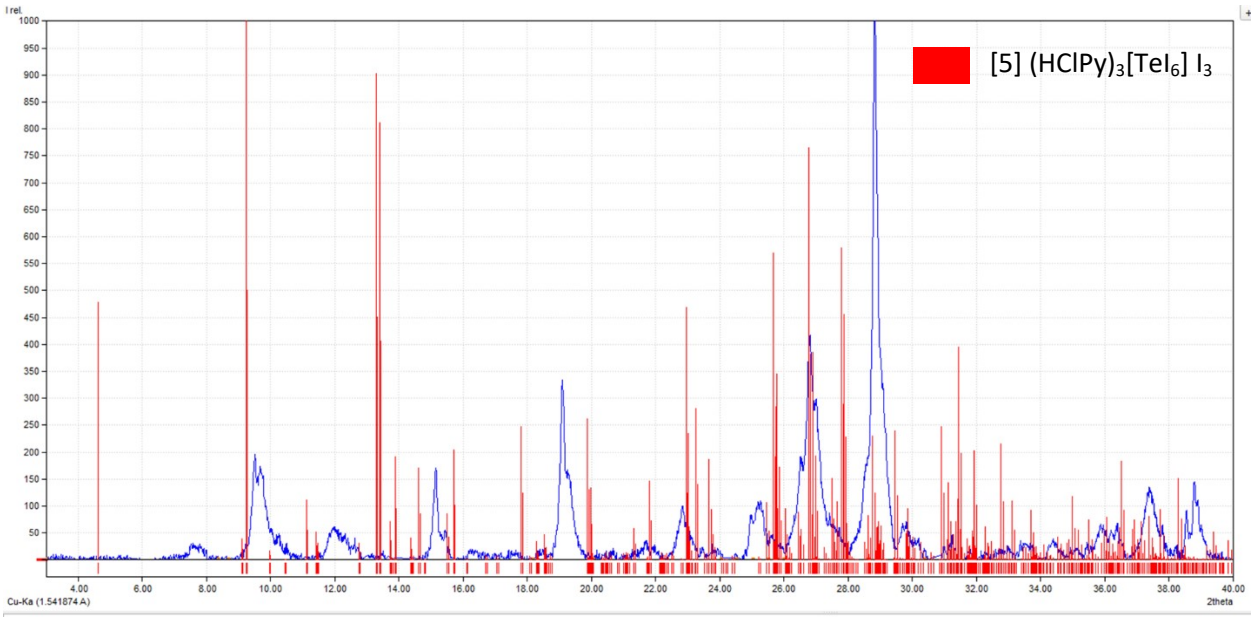

Figure S5. PXRD – 15 minutes after the synthesis of **5** $(HClPy)_3[TeI_6]\cdot I_3$. 15 minutes after mixing of reagents, very little if any of **5** is present, as seen from the mismatch of the calculated pattern of **5** in red. Solid products were filtered from liquid porition and dried before PXRD measurement.

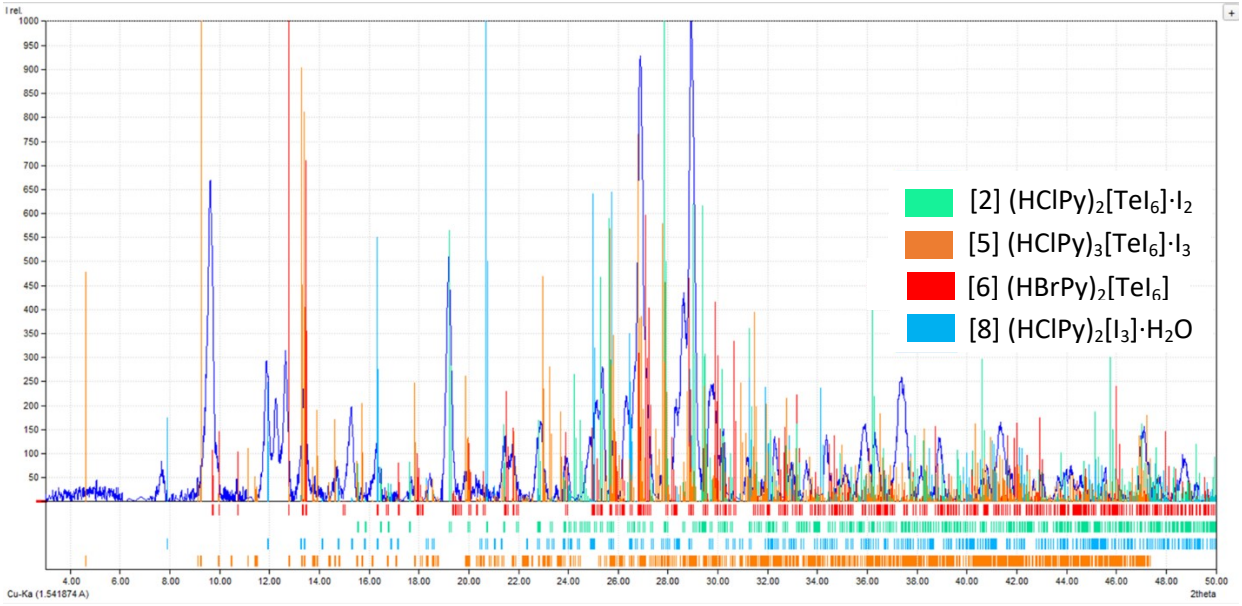

Figure S6. PXRD – 3 days after an attempted synthesis of **5**. After 3 days there is some in-growth of **5** (orange), but relatively little compared to various side products and impurities. For this reason, reliable DRS measurements for 5 couuld no be obtained.

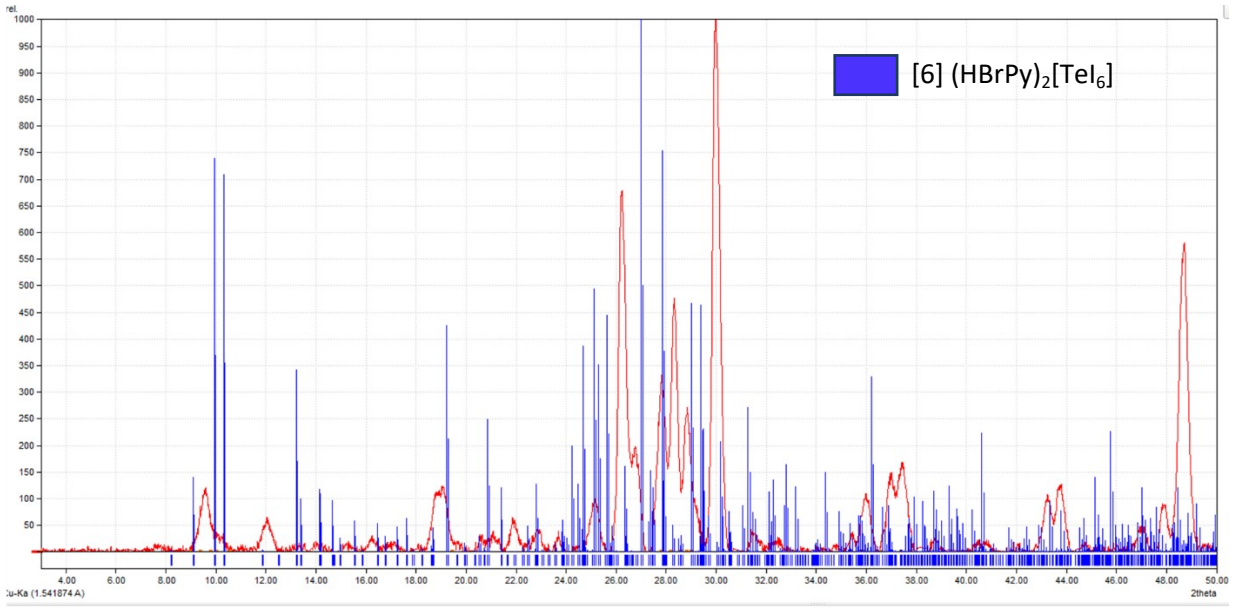

Figure S7. PXRD – 15 minutes after the synthesis of **6** $(HBrPy)_2[TeI_6]$. At this point, very little of **6** is actually present, as seen from the calculated pattern overlaid in blue. Solid products were filtered from the liquid portion and dried before PXRD measuremet.

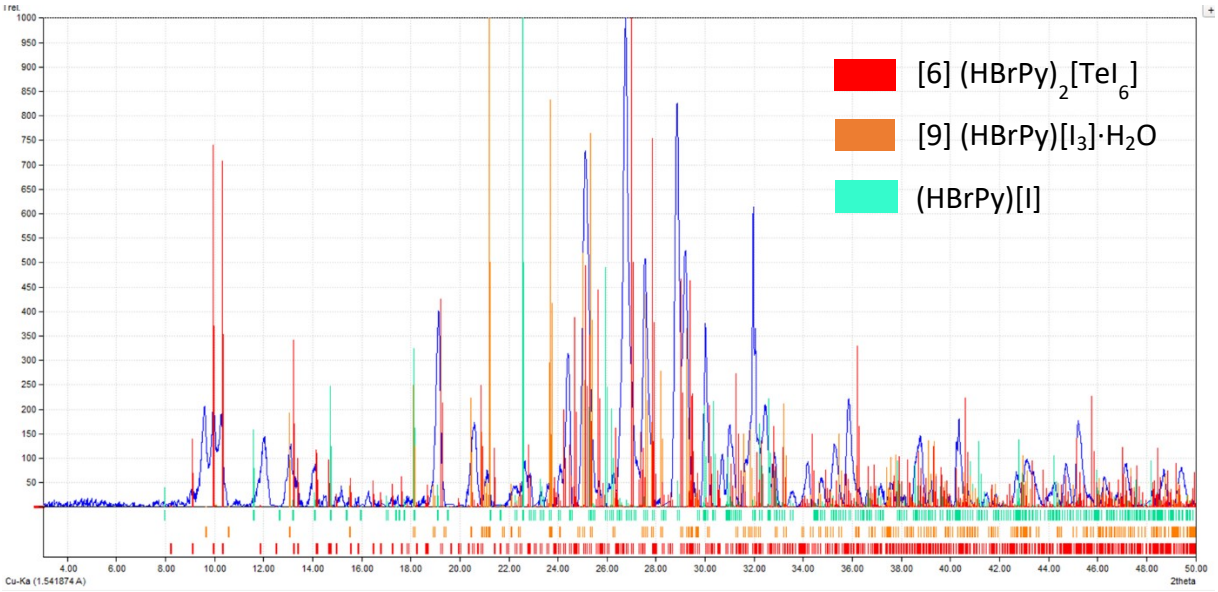

Figure S8. PXRD – 5 days after the synthesis of **6,** a significant amount has grown in as a solid phase (calculated pattern overlaid in red). Also present are the iodide and triiodide salts of BrPy.

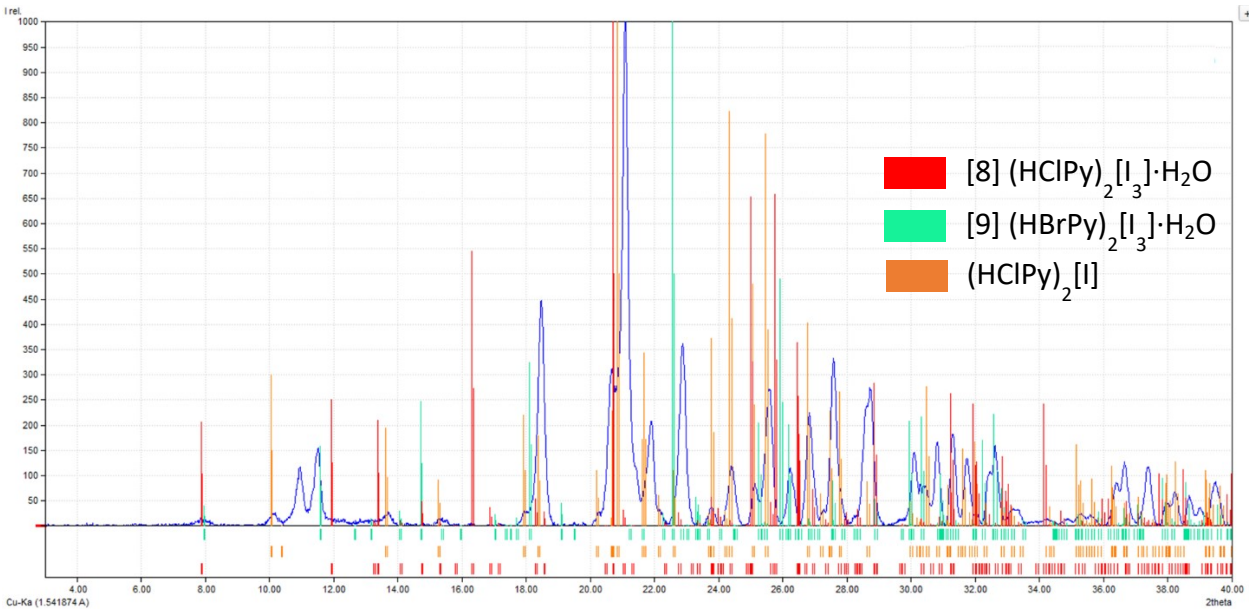

Figure S9. PXRD of **8** (HClPy)$[I_3]\cdot H_2O$ with the calculated pattern overlaid in red, and that of (HClPy)[I] overlaid in orange. The calculated pattern of **9** (HBrPy)$[I_3]\cdot H_2O$ can be seen in green, indicating there is a component of **8** structurally similar the monocolinic (space group C2/c (15)) compound **9**.

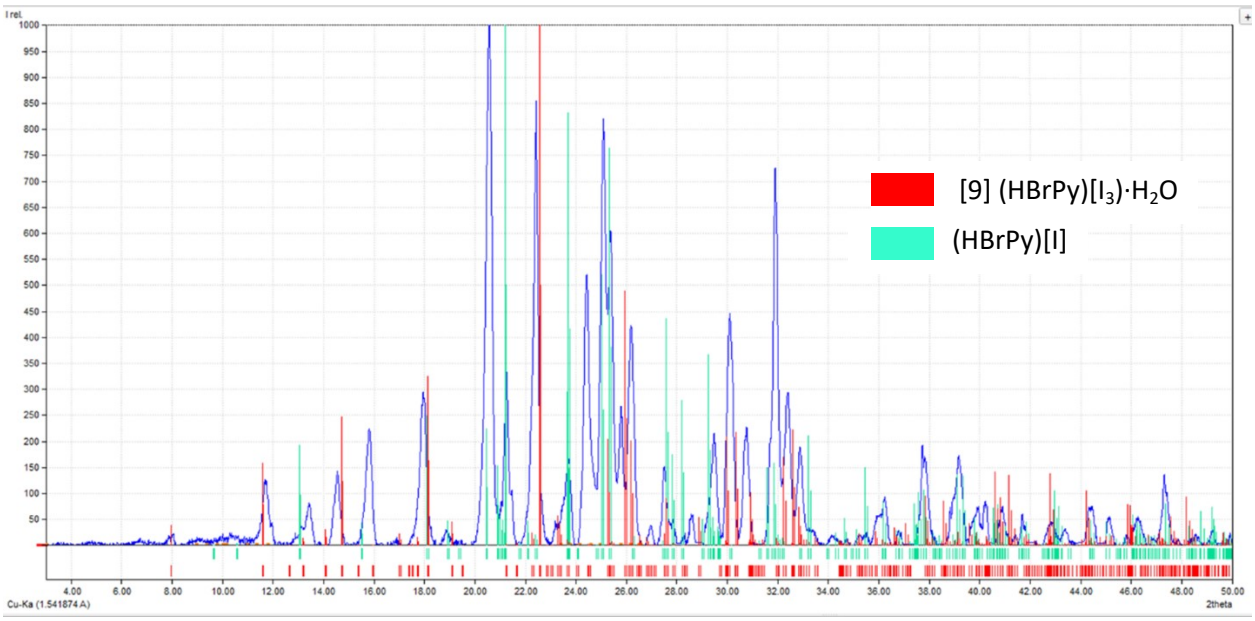

Figure S10. PXRD of **9** (HBrPy)[I_3]·H_2O overlaid with the calculated pattern for **9** and the HBrPy iodide salt in red and green respectively.

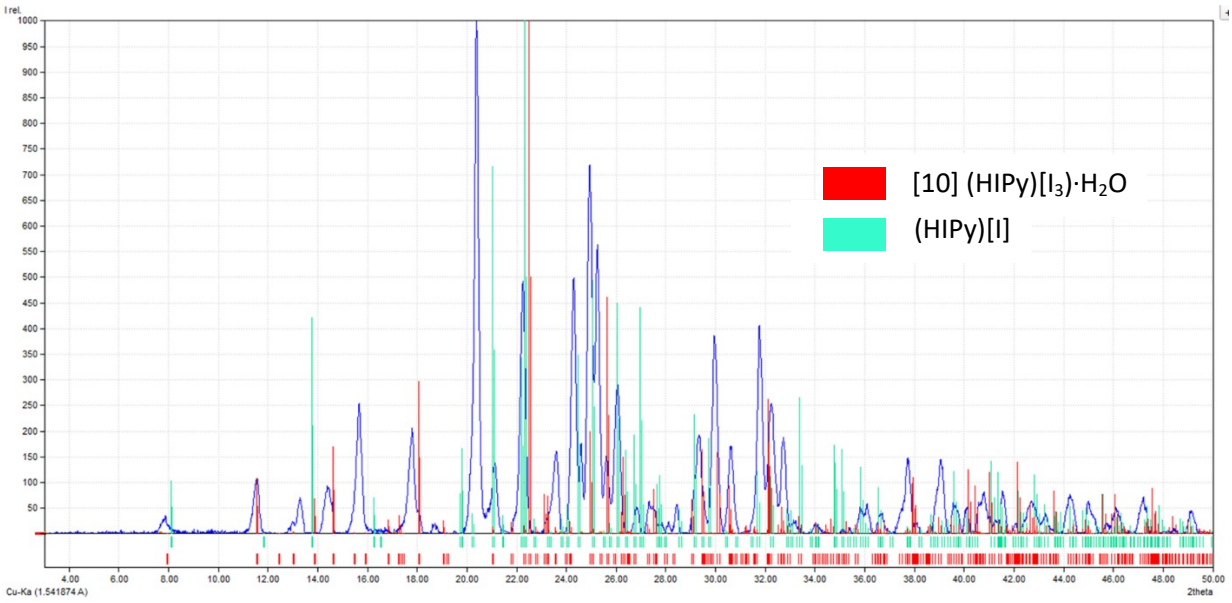

Figure S11. PXRD of **10** (HIPy)[I_3]·H_2O with the calculated pattern overlaid in red and (HIPy)[I] salt in green.

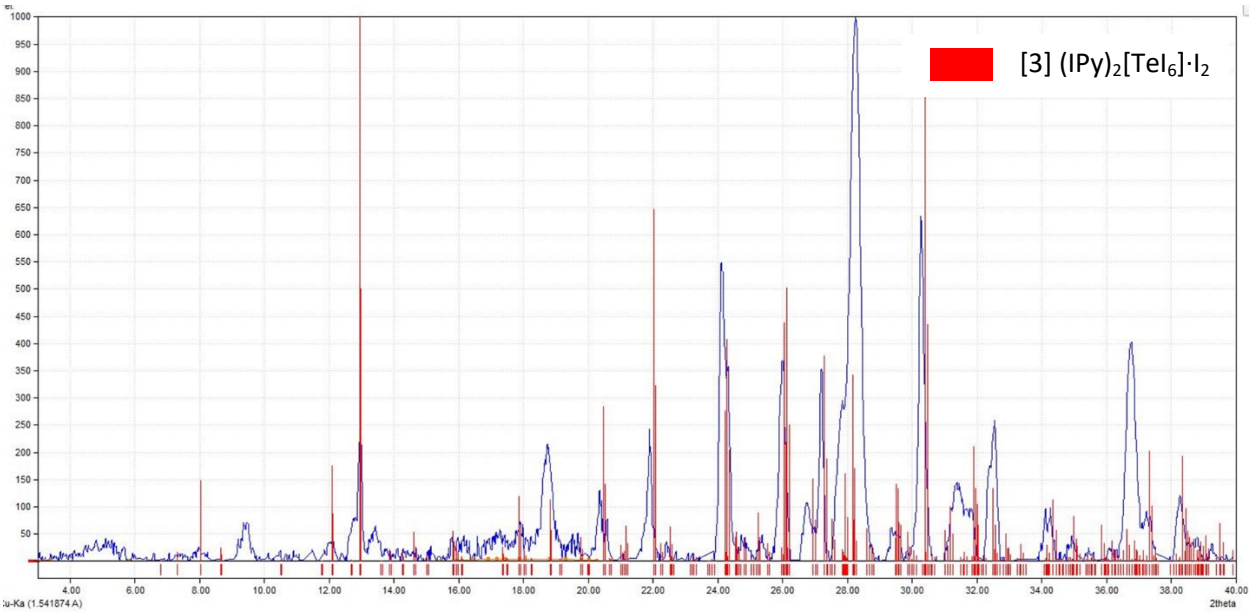

Figure S12. PXRD of synthesis attempting to make $(BrPy)_2[TeI_6]\cdot I_2$ (blue), overlaid with the calculated pattern of **3** ($(IPy)_2[TeI_6]\cdot I_2$), in red. This likely shows the presence of $(BrPy)_2[TeI_6]\cdot I_2$, nearly isomorphous with **3**.

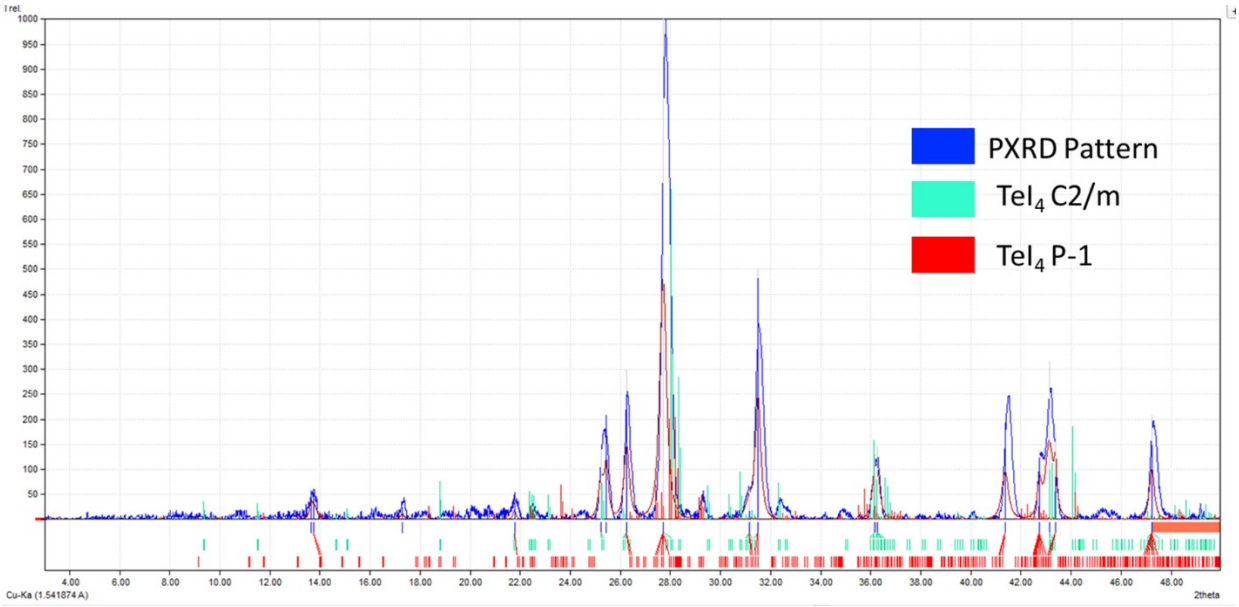

Figure S13. PXRD analysis of TeO_2 + HI after evaporating to dryness. The sample contains two main forms of TeI_4, whose calculated patterns are overlaid in red and green.

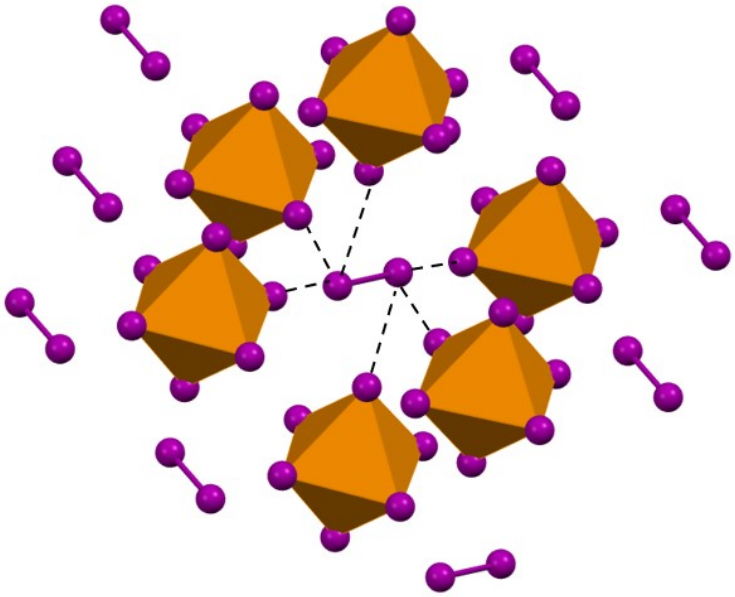

Figure S14. Extended structure of **1**, showing halogen bonding bewteen I_2 and surrounding $[TeI_6]^{2-}$, with HPy molecules omitted for clarity. This same second-sphere environment is present in **2** and **3**.

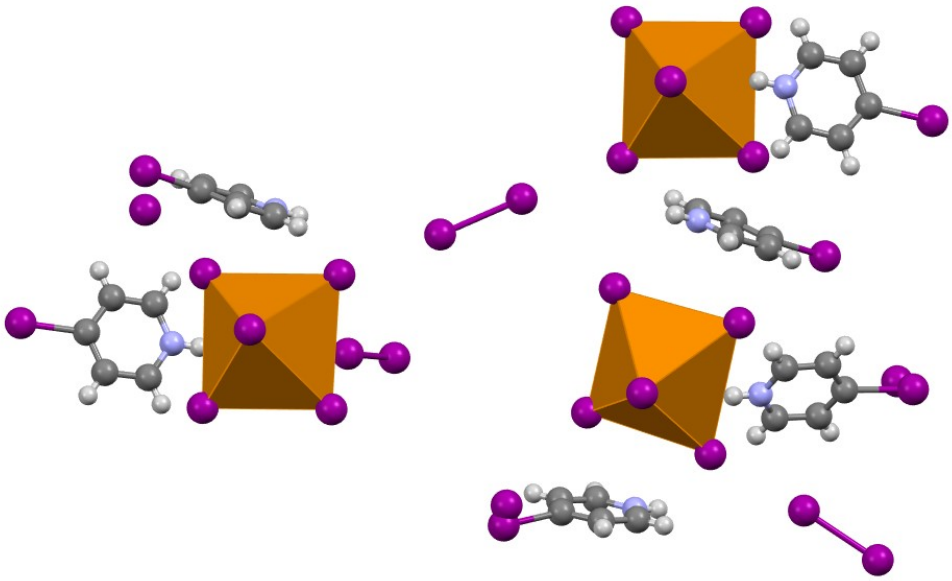

Figure S15: Asymmetric unit of **3**, with 3 crystallographically unique $[TeI_6]^{2-}$ octahedra and associated IPy (disordered) and I_2.

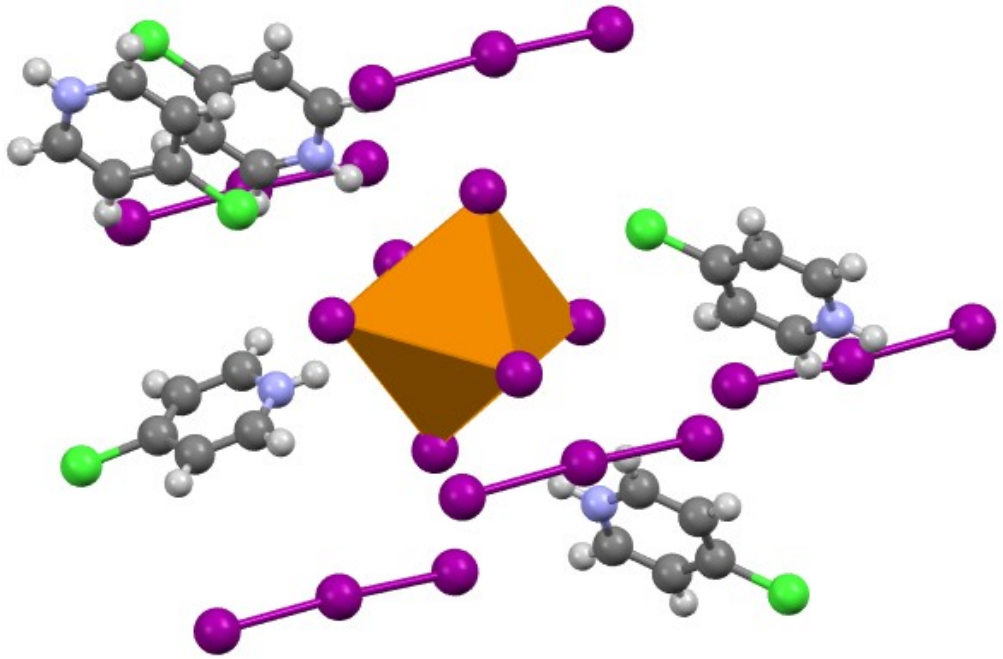

Figure S16. Second sphere environment of **5**, with nearest neighbor ClPy and I_3^- species. This is representative of the molecular model used for NBO single point energy calculations.

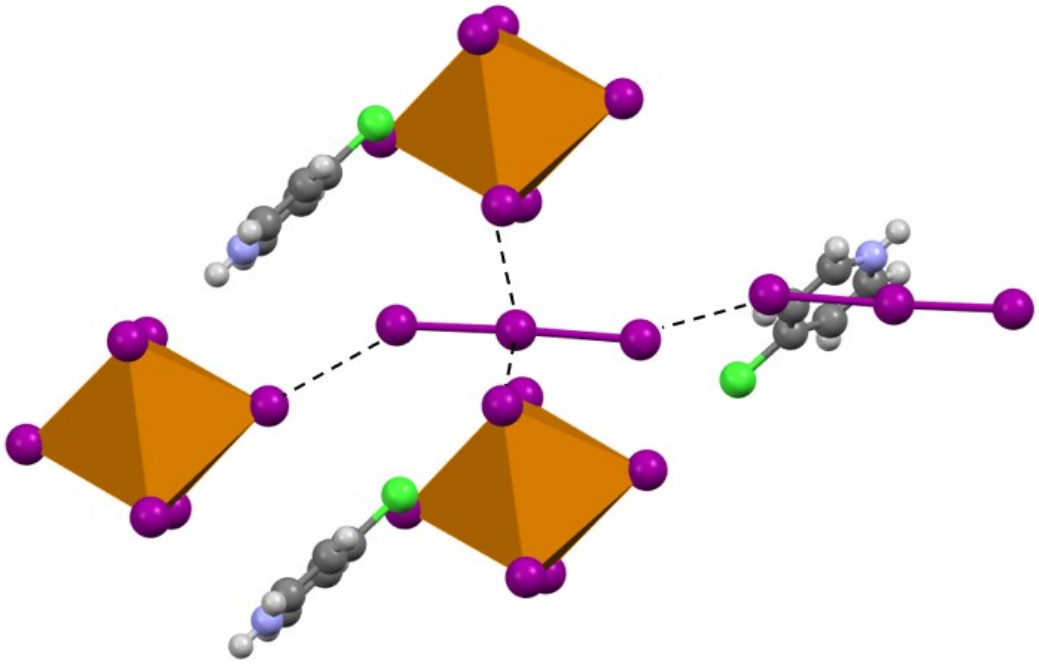

Figure S17. Halogen bonding interactions in **5** involving I_3^-. Each I_3^- interacts with 3 $[TeI_6]^{2-}$ and 1 other I_3^- via halogen bonding.

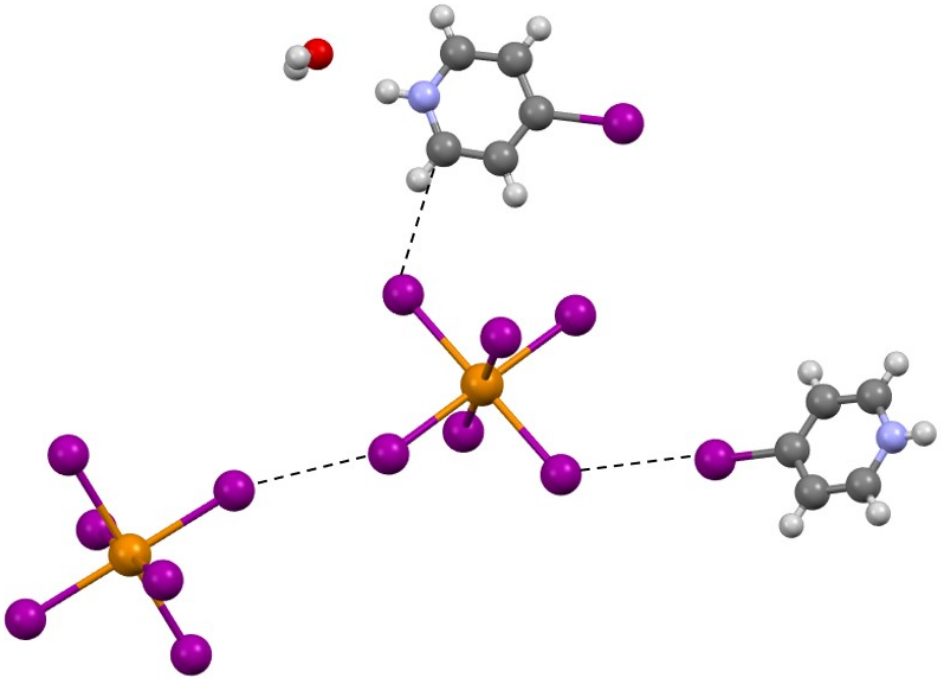

Figure S18. Non-covalent interactions in **7** $(HIPy)_2[TeI_6]\cdot H_2O$, including hydrogen and halogen bonding (dashed lines). Interactions between $[TeI_6]^{2-}$ octahedra are present as in **4**.

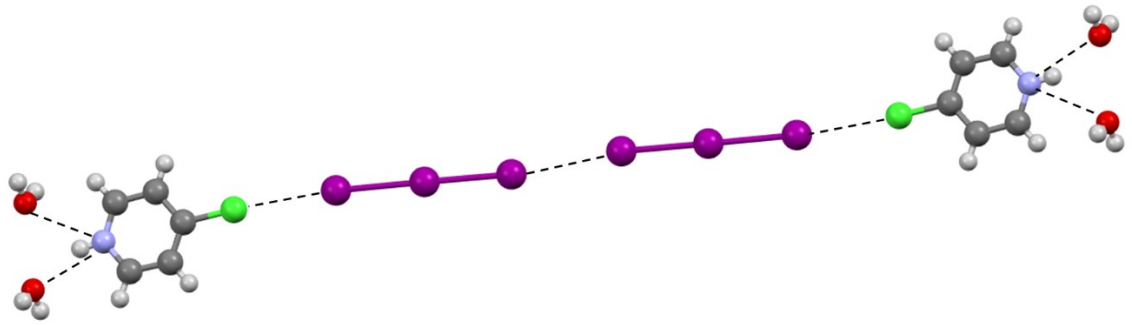

Figure S19. Coordination structure of **8-10**. This arrangements in 8-10 involves HXPy, I_3^-, and H_2O interacting via hydrogen and halogen bonding (dashed lines). **8** is isostructural with **9** and **10**.

	Interaction Type	Average Stabilization Energy, kcal/mol (single interaction)
1	side-on $[TeI_6]\cdots I_2$	4.84
2	side-on $[TeI_6]\cdots I_2$	2.97
3	side-on $[TeI_6]\cdots I_2$	4.43
4	n/a	n/a
5	side-on [TeI6]$\cdots I_3$	6.42
6	n/a	n/a

Table S1. Stabilization energy for side-on interactions in compounds **1-3**, and **4**. Stabilization energies are an average of the multiple side-on type interactions that occur between [TeI6]2- and I2. 4 and 6 do not contain side-on [TeI6]2-···I2 interactions comparable to those in 1-3, 4.

Stabilization Energies (kcal/mol) for HBrPy··$[TeI_6]^{2-}$ Noncovalent Interactions in 6			
Halogen Bond Donor (lone pairs)	**Hydrogen Bonding**	**Carbon Bonding**	**Halogen Bonding**
I2	0.47	1.17	0.9
I3	1.03	0.62	0.17
I4	3.36	4.92	0
I5	3.31	2.06	0
I6	1.22	1.57	0
I7	3.34	2.42	1.58
Totals	12.73	12.76	2.65

Table S2. Total NCI stabilization energies for **6**, sorted by type (hydrogen, carbon, and halogen bonding). Energies were extracted from an NBO single point energy calculation on a $[TeI_6]^{2-}$ octahedron surrounded by its 10 nearest neighbor BrPy cations. The interactions tabulated here arise from donation of a lone pair on a tellurium bound iodine into the σ* orbital of C-H or N-H bond (hydrogen bonding), a C-C or C-N (carbon bonding), or C-Br bond (halogen bonding). Hydrogen and carbon bonding clearly dominate over halogen bonding in terms of total stabilization energies.

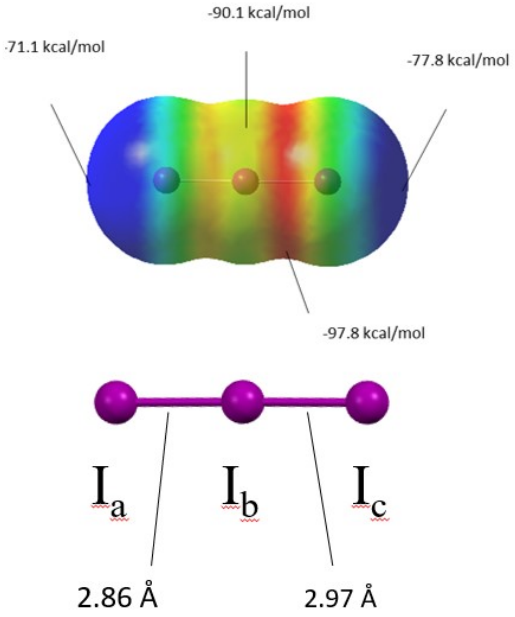

Figure S20. ESP and bond lengths an I_3^- molecule in **5**, specifically showing the asymmetric bond lengths within the I_3^- and resultant differences in electrostatic potential.

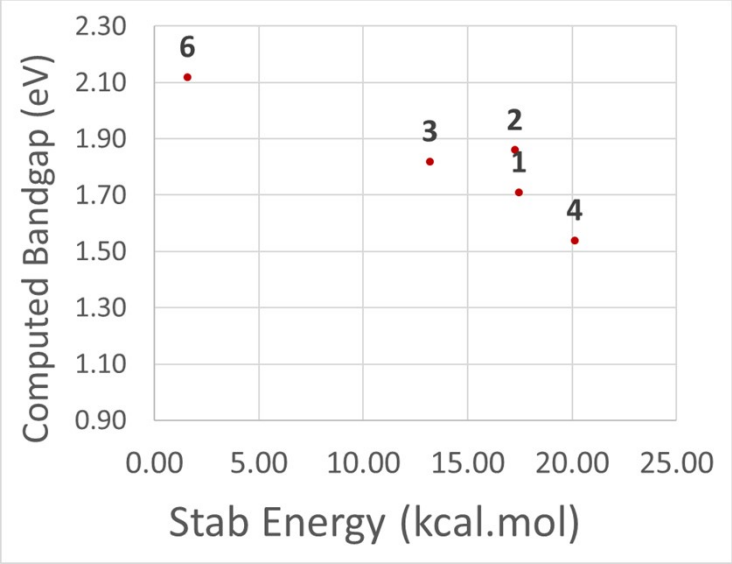

Figure S21. Plot of computationally derived bandgaps vs. stab. energy for **1-4**, **6**.

Elemental Analysis Results							
Compound 1		**$(HPy)_2[TeI_6] \bullet I_2$**		**Compound 6**		**$(HBrPy)_2[TeI_6]$**	
Element	Theory (%)	Trial 1	Trial 2	Element	Theory(%)	Trial 1	Trial 2
C	9.22	9.69	9.79	C	9.95	12.02	11.96
H	0.93	0.97	1.03	H	0.84	1.16	1.02
N	2.15	2.28	2.21	N	2.32	2.80	2.72
I	77.91	67.23		I	63.08	52.89	
Compound 2		**$(HClPy)_2[TeI_6] \bullet I_2$**		**Compound 7**		**$(HIPy)_2[TeI_6]\cdot H_2O$**	
Element	Theory (%)	Trial 1	Trial 2	Element	Theory (%)	Trial 1	Trial 2
C	8.75	8.14	8.03	C	9.11	0.11	0.20
H	0.73	0.79	0.81	H	0.92	0.77	0.73
N	2.04	1.89	1.82	N	2.12	0.00	0.00
I	74.00	69.63		I	76.97	67.42	
Compound 3		**$(HIPy)_2[TeI_6] \bullet I_2$**		**Compound 8**		**$(HClPy)[I_3]\cdot H_2O$**	
Element	Theory (%)	Trial 1	Trial 2	Element	Theory (%)	Trial 1	Trial 2
C	7.72	8.16	8.26	C	11.70	15.55	15.47
H	0.65	0.87	0.92	H	1.37	1.59	1.56
N	1.80	1.73	1.64	N	2.73	3.63	3.58
I	81.20	75.03		I	74.17	52.54	
Compound 4		**$(Pyz)_2[TeI_6] \bullet 2I_2$**		**Compound 9**		**$(HBrPy)[I_3]\cdot H_2O$**	
Element	Theory (%)	Trial 1	Trial 2	Element	Theory (%)	Trial 1	Trial 2
C	7.59	6.22	6.17	C	10.77	12.07	11.93
H	0.64	0.59	0.52	H	1.27	1.67	1.52
N	3.54	3.52	3.46	N	2.51	2.81	2.69
I	80.17	78.81		I	68.26	57.15	
Compound 5		**$(HClPy)_3[TeI_6] \bullet I_3$**		**Compound 10**		**$(HIPy)[I_3]\cdot H_2O$**	
Element	Theory (%)	Trial 1	Trial 2	Element	Theory (%)	Trial 1	Trial 2
C	11.17	11.10		C	9.93	11.78	11.83
H	0.94	1.00		H	1.17	1.52	1.48
N	2.60	2.58		N	2.32	2.72	2.64
I	70.69	70.51		I	83.94	77.44	

Table S3: Results of elemental analysis reported as % mass. See table S4 for weight % of common impurities in 1-10.

Common Impurities				
TeI_4			**$(HClPy)[I_3]\cdot H_2O$**	
Element	Theory (%)		Element	Theory (%)
C	0.00		C	11.70
H	0.00		H	1.37
N	0.00		N	2.73
I	70.91		I	74.17
ClPy I-			**$(HBrPy)[I_3]\cdot H_2O$**	
Element	Theory (%)		Element	Theory (%)
C	24.87		C	10.77
H	2.09		H	1.27
N	5.80		N	2.51
I	52.56		I	68.26
BrPy I-			**$(HIPy)[I_3]\cdot H_2O$**	
Element	Theory (%)		Element	Theory (%)
C	21.00		C	9.93
H	1.76		H	1.17
N	4.90		N	2.32
I	44.39		I	83.94
IPy I-				
Element	Theory (%)			
C	18.04			
H	1.51			
N	4.21			
I	76.24			

Table S4: Theoretical % mass for common impurities in 1-10. The presence of these impurities, as identified by PXRD, and the loss of I_2 can account for discrepancies between theory and experimental values for C, H, N, and I in Table S3.